Error Sources

✓ Errors in the detection mechanism can arise from various noises and disturbances associates with the signal detection system.

✓ The two most common samples of the spontaneous fluctuations are shot noise and thermal noise.

✓ Shot noise arises in electronic devices because of the discrete nature of current flow in the device.

✓ Thermal noise arises from the random motion of electrons in a conductor.

✓ The random arrival rate of signal photons produces a quantum (or shot) noise at the photodetector. This noise depends on the signal level.

✓ This noise is of particular importance for PIN receivers that have large optical input levels and for APD receivers.

✓ When using an APD, an additional shot noise arises from the statistical nature of the multiplication process. This noise level increases with increasing avalanche gain *M*.

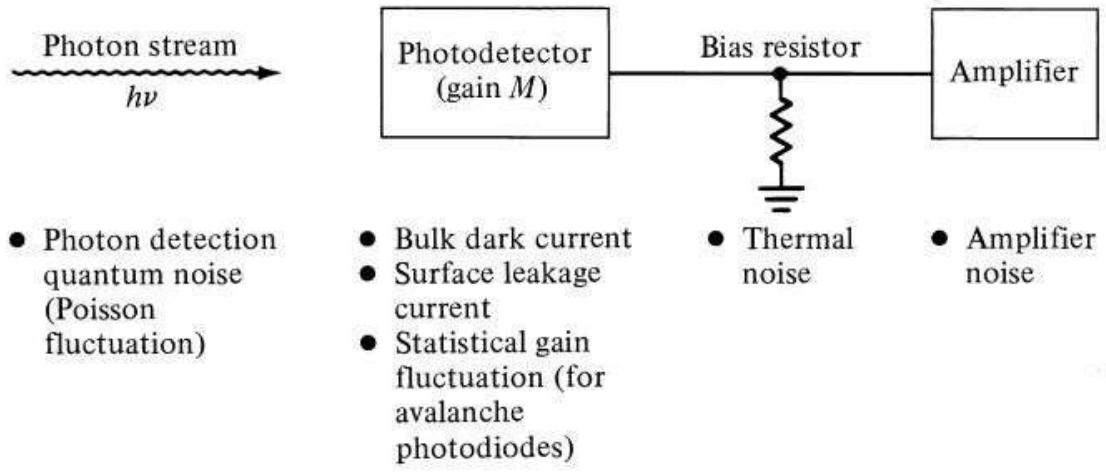

Figure 4.2 Noise sources and disturbances in the optical pulse detection mechanism.

[Source: htpp://img.brainkart.com]

✓ Thermal noises arising from the detector load resistor and from the amplifier electronics tend to dominate in applications with low SNR when a PIN photodiode is used.

✓ When an APD is used in low-optical-signal level applications, the optimum avalanche gain is determined by a design tradeoff between the thermal noise and the gain-dependent quantum noise.

✓ The primary photocurrent generated by the photodiode is a time-varying Poisson process.

✓ If the detector is illuminated by an optical signal $P(t)$, then the average number of electron-hole pairs generated in a time t is

$$\overline{N} = \frac{\eta}{h\nu}\int_0^t P(t)dt = \frac{\eta E}{h\nu}$$

where h is the detector quantum efficiency, *h*n is the photon energy, and E is the energy received in a time interval .

✓ The actual number of electron-hole pairs n that are generated fluctuates from the average according to the Poisson distribution

$$P_r(n) = \overline{N}^n \frac{e^{-\overline{N}}}{n!}$$

where Pr(n) is the probability that n electrons are emitted in an interval t

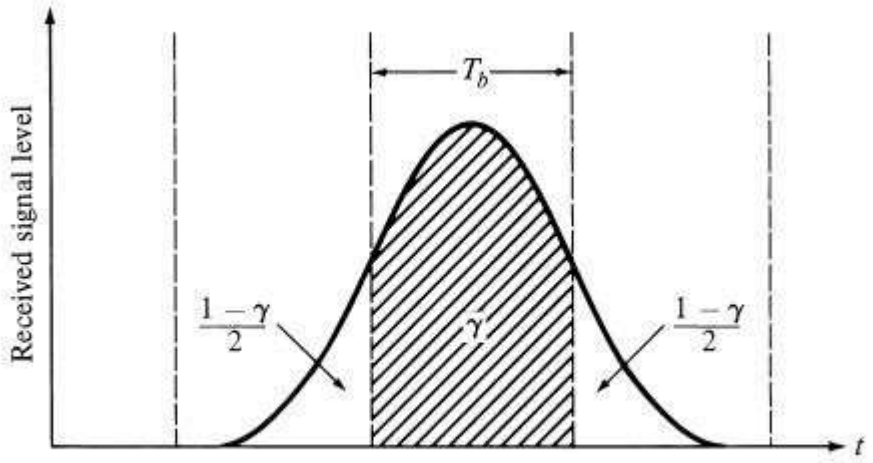

Figure 4.3 Pulse spreading in an optical signal that leads to ISI.

[Source: htpp://img.brainkart.com]

✓ For a detector with a mean avalanche gain M and an ionization rate ratio k, the excess noise factor $F(M)$ for electron injection is where the factor x ranges between 0 and 1.0 depending on the photodiode material.

$$F(M) = kM + \left(2 - \frac{1}{M}\right)(1-k)$$

Or

$$F(M) \cong M^x$$

✓ A further error source is attributed to *intersymbol interference* (ISI), which results from pulse spreading in the optical fiber.

✓ The fraction of energy remaining in the appropriate time slot is designated by so that 1-g is the fraction of energy that has spread into adjacent time slots.

Receiver Configuration

✓ A typical optical receiver is shown in Figure 4.4. The three basic stages of the receiver are a photodetector, an amplifier, and an equalizer.

✓ The photo-detector can be either an APD with a mean gain M or a PIN for which M=1.

✓ The photodiode has a quantum efficiency h and a capacitance Cd.

✓ The detector bias resistor has a resistance Rb which generates a thermal noise current ib(t).

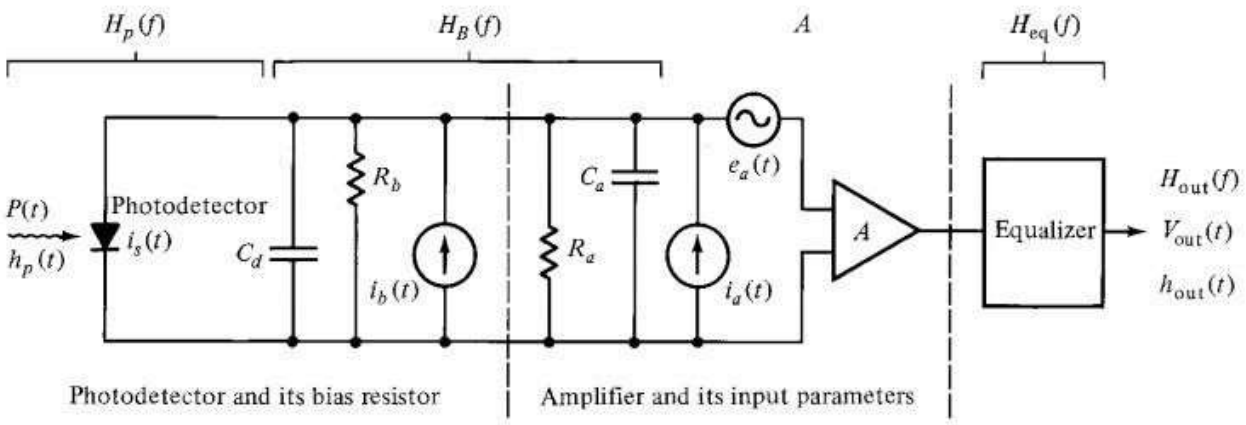

Figure 4.4 Schematic diagram of a typical optical receiver.

[Source: htpp://img.brainkart.com]

Amplifier Noise Sources:

✓ The input noise current source *ia*(*t*) arises from the thermal noise of the amplifier input resistance *R*a;

✓ The noise voltage source *ea*(*t*) represents the thermal noise of the amplifier channel.

✓ The noise sources are assumed to be Gaussian in statistics, flat in spectrum (which characterizes *white* noise), and uncorrelated (statistically independent).

The Linear Equalizer:

✓ The equalizer is normally a linear frequency shaping filter that is used to mitigate the effects of signal distortion and inter symbol interference (ISI).

✓ The equalizer accepts the combined frequency response of the transmitter, the fiber, and the receiver, and transforms it into a signal response suitable for the following signal processing electronics.

✓ The binary digital pulse train incident on the photo-detector can be described by

$$P(t) = \sum_{n=-\infty}^{\infty} b_n h_p(t - nT_b)$$

✓ Here, $P(t)$ is the received optical power, Tb is the bit period, bn is an amplitude parameter representing the nth message digit, and hp(t) is the received pulse shape.

✓ Let the nonnegative photodiode input pulse hp(t) be normalized to have unit area

$$\int_{-\infty}^{\infty} h_p(t)dt = 1$$

then bn represents the energy in the nth pulse.

✓ The mean output current from the photodiode at time t resulting from the pulse train given previously is

$$\langle i(t) \rangle = \frac{\eta q}{h\nu} MP(t) = R_0 \sum_{n=-\infty}^{\infty} b_n h_p(t - nT_b)$$

where Ro = hq/hn is the photodiode responsivity.

✓ The above current is then amplified and filtered to produce a mean voltage at the output of the equalizer.

PROBABLITY OF ERROR

- The digital receiver performance can be evolved by measuring of error and quantum limit.
- In practice, several standard ways are available to measuring the rate of error occurrences in a digital data stream.

- **Bit error rate or the error rate [BER]**

Bit error rate is defined by the ratio between number of errors (Ne) occurring over a certain time interval t to the number of error (Nt) during this interval.

$$BER = \frac{N_e}{N_t} = \frac{N_e}{B_t}$$

Where $B=1/T_b$ is the bit rate (is the pulse transmission rate).

- The error rates the optical fiber telecommunication system range from 10^{-9} to 10^{-12}.
- The probability distribution of signal at the equalizer output should be known to compute BER. Here the decision is made as to whether a 0 or a 1 is sent.

$$P_1(v) = \int_{-\infty}^{v} p(y/1)dy$$

$$P_0(v) = \int_{v}^{\infty} p(y/0)dy$$

P_1 (v) is the probability that the equalizer output voltage is less than v when log"1" is sent.

P_0 (v) is the probability that the equalizer output voltage exceeds "v" when logic 'o' is sent.

- The figure shows the probability distribution for received logic 0 and 1.The function P(y/1) and P(y/0) are the conditional probability distribution functions, that is P(y/x) is the probability that the output voltage is y, given that an x was transmitted.
- If the threshold voltage is v_{th} then the error probability P_e is defined as

$$P_e = a\,P_1(v_{th}) + b\,P_0(v_{th})$$

- The weighing factors a and b determined by the priori distribution of the data and b are the probabilities that either a 1 or 0 occurs.
- To calculate the "p_e", the mean and standard deviation of the output voltage V_{out} (t) should be known.
- Thus, let us assume that a signal S (Which can be either a noise disturbance or a desired information bearing signal) has a Gaussian probability distribution function with a mean value m.

$$f(s)\,ds = \frac{1}{\sqrt{2\pi\sigma^2}}\, e^{-(s-m)^2/2\sigma^2} \cdot ds$$

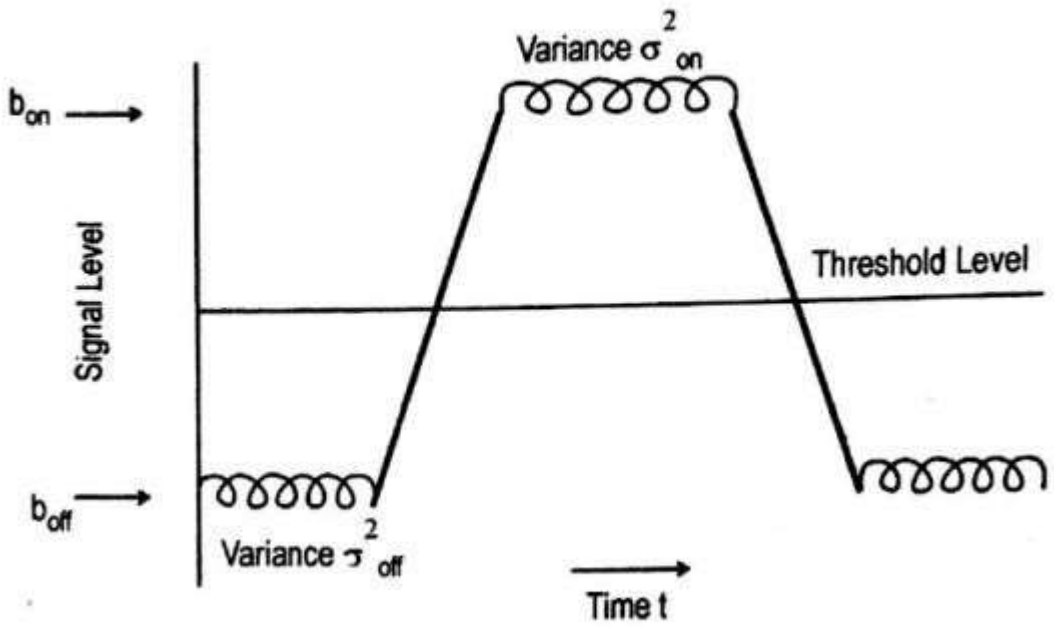

Figure 4.5 Gaussian Noise Statistics of a Binary Signal

[Source: htpp://img.brainkart.com]

- Now, we can use the probability density function to determine the probability of error for a data stream in which the 1 pulse are all of amplitude V.
- The above figure shows, the mean and variance of the Gaussian output for a 1 pulse are b_{on} and σ_{on2}, respectively, whereas for a 0 pulse they are b_{off} and σ_{off2}, respectively.

PROBABILITY OF ERROR WHEN 0 PULSE SENT

- Let us first consider the case of o pulse being sent. So that no pulse is present at the decoding time. The probability that noise will exceed the threshold voltage v_{th} and be 1 pulse.

$$P_0(v_{th}) = \int_{v_{th}}^{\infty} p(y/0)dy = \int_{v_{th}}^{\infty} f_0(y)dy$$

$$= \frac{1}{\sqrt{2\pi}\,\sigma_{off}} \int_{v_{th}}^{\infty} \exp\left[-\frac{(v-b_{off})^2}{2\sigma_{off}^2}\right] dv$$

- Where the subscript 0 denotes the presence of a 0 bit.

PROBABILITY OF ERROR WHEN 1 PULSE SENT

- Transmitted pulse 1 is misinterpreted as a o by the electronics following the equalizer.

$$P_1(v_{th}) = \int_{-\infty}^{v_{th}} p(y/1)dy = \int_{-\infty}^{v_{th}} f_1(v)dv$$

$$= \frac{1}{\sqrt{2\pi}\,\sigma_{on}} \int_{-\infty}^{v_{th}} \exp\left[-\frac{(b_{on}-v)^2}{2\sigma_{on}^2}\right] dv$$

Where the subscript 1 denotes the presence of a 1 bit.

QUANTUM LIMIT

- An ideal photodetector which has unity quantum efficiency and which produces no dark current, that is no electron holde pairs are generated in the absence of an optical pulse.

- This condition, it is possible to find the minimum received optical power required for a specific nit error rate performance in a digital syatem. This minimum received power level is known as the quantum limit.

- Assume an optical pulse of energy E falls on the photodeetector in a time interval τ. This can only be interpreted by the receiver as a 0 pulse if no electron hole pairs are generated with the pulse with the pulse present.

- The probability that n=0 electrons are emitted in a time interval τ is

$$P_r(o) = e^{-\overline{N}}$$

where the average number of electron-hole pairs, $\overline{N} = \eta E / hv$.

- Thus for a given probability $P_r(o)$, we can find the minimum energy E required at a specific wavelength λ.

Fiber Measurements

1. Fiber Attenuation Measurements

Fiber attenuation measurement techniques have been developed in order to determine the total fiber attenuation of the relative contributions to this total from both absorption losses and scattering losses. The overall fiber attenuation is of greatest interest to the system designer, but the relative magnitude of the different loss mechanisms is important in the development and fabrication of low-loss fibers. Measurement techniques to obtain the total fiber attenuation give either the spectral loss characteristic or the loss at a single wavelength (spot measurement).

A commonly used technique for determining the total fiber attenuation per unit length is the cut-back or differential method. Figure 4.5 shows a schematic diagram of the typical experimental setup for measurement of the spectral loss to obtain the overall attenuation spectrum for the fiber. It consists of a 'white' light source, usually a tungsten halogen or xenon are lamp. The focused light is mechanically chopped at a low frequency of a few hundred hertz. This enables the lock-in amplifier at the receiver to perform phase-sensitive detection.

The chopped light is then fed through a monochromator which utilizes a prism or diffraction grating arrangement to select the required wavelength at which the attenuation is to be measured. Hence the light is filtered before being focused onto the fiber by means of a microscope objective lens. A beam splitter may be incorporated before the fiber to provide light for viewing optics and a reference signal used to compensate for output power fluctuations.

When the measurement is performed on multimode fibers it is very dependent on the optical launch conditions. Therefore unless the launch optics are arranged to give the steady-state mode distribution at the fiber input, or a dummy fiber is used, then a mode scrambling device is attached to the fiber within the first meter.

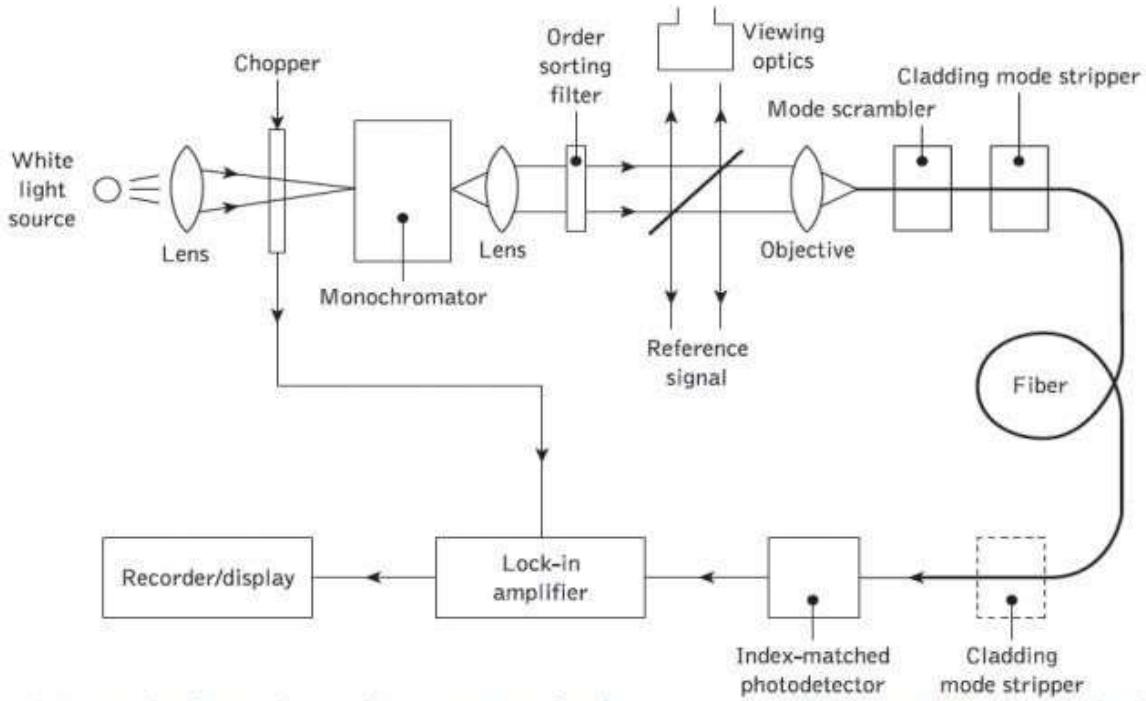

Figure 4.5 A typical experimental arrangement for the measurement of spectral loss in optical fibers using the cut-back technique

[Source: htpp://img.brainkart.com]

The fiber is also usually put through a cladding mode stripper, which may consist of an S-shaped groove cut in the Teflon and filled with glycerine. This device removes light launched into the fiber cladding through radiation into the index-matched (or slightly higher refractive index) glycerine. A mode stripper can also be included at the fiber output end to remove any optical power which is scattered from the core into the cladding down the fiber length. This tends to be pronounced when the fiber cladding consists of a low-refractive-index silicone resin.

The optical power at the receiving end of the fiber is detected using a *p–i–n* or avalanche photodiode. In order to obtain reproducible results the

photodetector surface is usually index matched to the fiber output end face using epoxy resin or an index-matching gell. Finally, the electrical output from the photodetector is fed to a lock-in amplifier, the output of which is recorded.

The cut-back method* involves taking a set of optical output power measurements over the required spectrum using a long length of fiber (usually at least a kilometer). This fiber is generally uncabled having only a primary protective coating. Increased losses due to cabling do not tend to change the shape of the attenuation spectrum as they are entirely radiative, and for multimode fibers are almost wavelength independent.

The fiber is then cut back to a point 2 m from the input end and, maintaining the same launch conditions, another set of power output measurements is taken.

$$\alpha_{dB} = \frac{10}{L_1 - L_2} \log_{10} \frac{P_{02}}{P_{01}}$$

$L1$ and $L2$ are the original and cut-back fiber lengths respectively, and $P01$ and $P02$ are the correspondingoutput optical powers at a specific wavelength from the original and cut-back fiber lengths. Hence when $L1$ and $L2$ are measuredin kilometers, αdB has units of dB km^{-1}.

$$\alpha_{dB} = \frac{10}{L_1 - L_2} \log_{10} \frac{V_2}{V_1}$$

where $V1$ and $V2$ correspond to output voltage readings from the original fiber length and the cut-back fiber length respectively.

2. Fiber Absorption Loss Measurement

It was indicated in the preceding section that there is a requirement for the optical fiber manufacturer to be able to separate the total fiber attenuation into the contributions from the major loss mechanisms. Material absorption loss measurements allow the level of impurity content within the fiber material to be checked in the manufacturing process.

The measurements are based on calorimetric methods which determine the temperature rise in the fiber or bulk material resulting from the absorbed optical energy within the structure. The apparatus shown in Figure 4.6, which is used to measure the absorption loss in optical fibers, was modified from an earlier version which measured the absorption losses in bulk glasses. This temperature measurement technique, illustrated diagrammatically in Figure 4.6(b), has been widely adopted for absorption loss measurements.

The two fiber samples shown in Figure 4.6(b) are mounted in capillary tubes surrounded by a low-refractive-index liquid (e.g. methanol) for good electrical contact, within the same enclosure of the apparatus shown in Figure 4.6(a). A thermocouple is wound around the fiber containing capillary tubes using one of them as a reference junction (dummy fiber).

Light is launched from a laser source (Nd : YAG or krypton ion depending on the wavelength of interest) through the main fiber (not the dummy), and the temperature rise due to absorption is measured by the thermocouple and indicated on a nanovoltmeter. Electrical calibration may be achieved by replacing the optical fibers with thin resistance wires and by passing known

electrical power through one. Independent measurements can then be made using the calorimetric technique and with electrical measurement instruments.

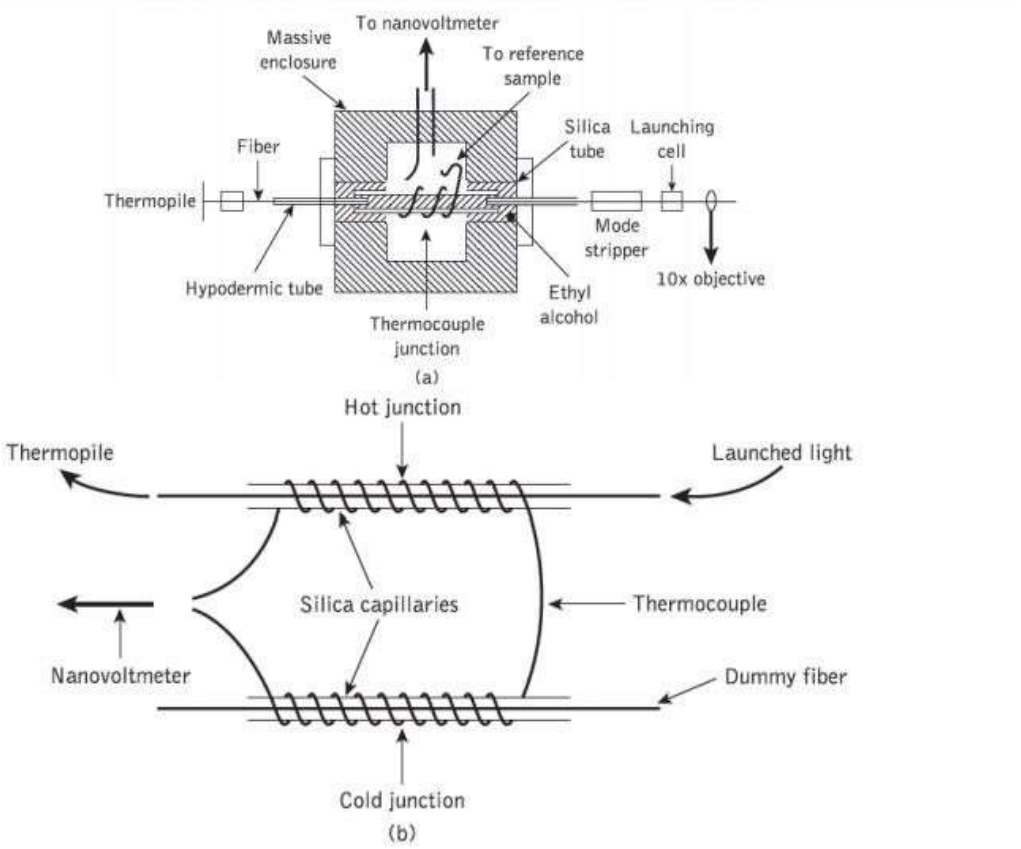

Figure 4.6 Calorimetric measurement of fiber absorption losses: (a) schematic diagram of a version of the apparatus; (b) the temperature measurement technique using a thermocouple

[Source: htpp://img.brainkart.com]

The calorimetric measurements provide the heating and cooling curve for the fiber sample used. A typical example of this curve is illustrated in Figure 4.7(a). The attenuation of the fiber due to absorption αabs may be determined from this heating and cooling characteristic. A time constant *t*c can be obtained from a plot of (*T*∞-*Tt*) on a logarithmic scale against the time *t*, an example of which shown in Figure 4.7(c) was obtained from the heating characteristic displayed in Figure 4.7(b). *T*∞ corresponds to the maximum temperature rise of the fiber under test and *Tt* is the temperature rise at a time *t*.

It may be observed from Figure 4.7(a) that $T\infty$ corresponds to a steady-state temperature for the fiber when the heat loss to the surroundings balances the heat generated in the fiber resulting from absorption at a particular optical power level. The time constant tc may be obtained from the slope of the straight line plotted in Figure 4.7(c) as:

$$t_c = \frac{t_2 - t_1}{\ln(T_\infty - T_{t_1}) - \ln(T_\infty - T_{t_2})} \tag{14.3}$$

$$\alpha_{abs} = \frac{CT_\infty}{P_{opt} t_c} \text{ dB km}^{-1} \tag{14.4}$$

where C is proportional to the thermal capacity per unit length of the silica capillary and the low-refractive-index liquid surrounding the fiber, and Popt is the optical power propagating in the fiber under test. The thermal capacity per unit length may be calculated, or determined by the electrical calibration utilizing the thin resistance wire.

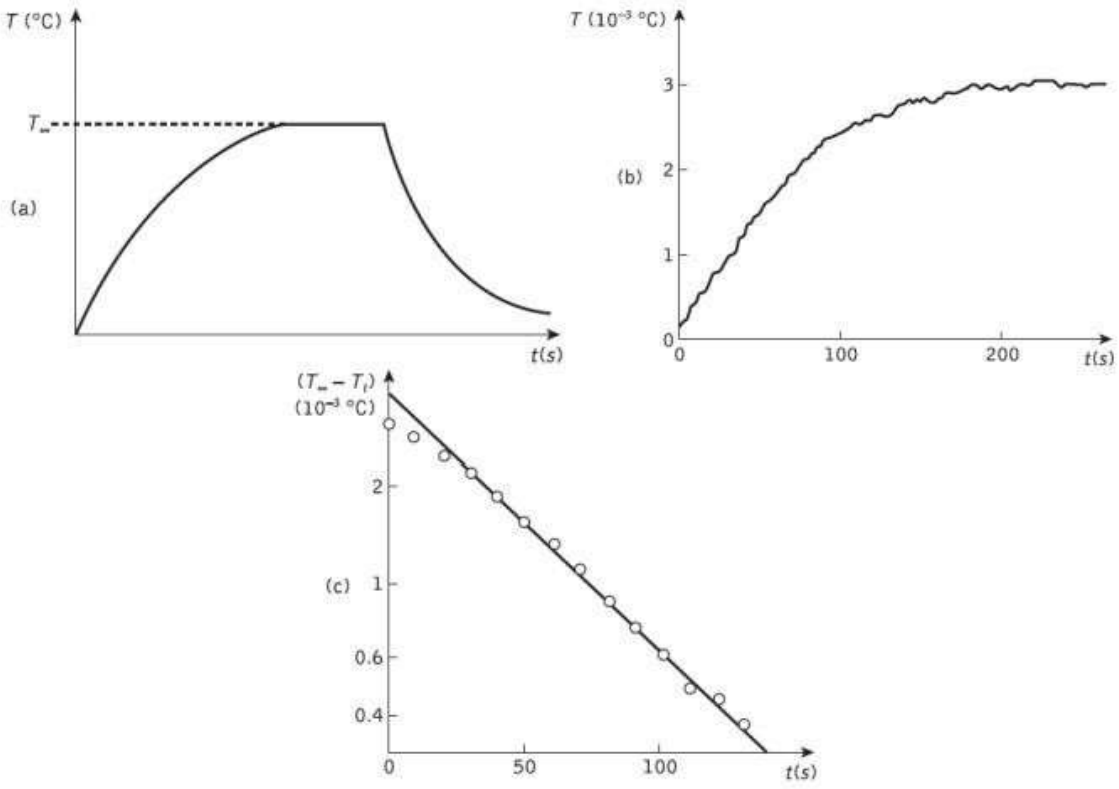

Figure 4.7 (a) A typical heating and cooling curve for a glass fiber sample. (b) A heating curve. (c) The corresponding plot of ($T\infty - Tt$) against time for a sample glass rod

3. Fiber Scattering Loss Measurement

The usual method of measuring the contribution of the losses due to scattering within the total fiber attenuation is to collect the light scattered from a short length of fiber and compare it with the total optical power propagating within the fiber.

Light scattered from the fiber may be detected in a scattering cell as illustrated in the experimental arrangement shown in Figure 4.8. This may consist of a cube of six square solar cells or an integrating sphere and detector. The solar cell cube which contains index-matching fluid surrounding the fiber gives measurement of the scattered light, but careful balancing of the detectors is required in order to achieve a uniform response.

This problem is overcome in the integrating sphere which again usually contains indexmatching fluid but responds uniformly to different distributions of scattered light. However, the integrating sphere does exhibit high losses from internal reflections. Other variations of the scattering cell include the internally reflecting cell and the sandwiching of the fiber between two solar cells.

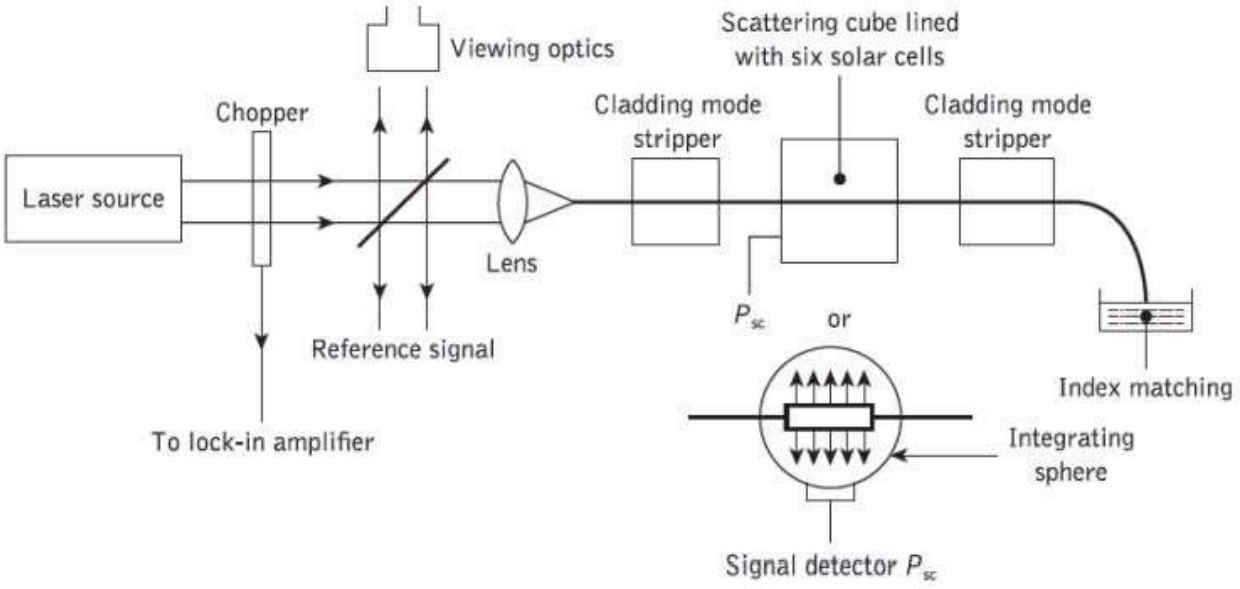

Figure 4.8 An experimental setup for measurement of fiber scattering loss illustrating both the solar cell cube and integrating sphere scattering cells

[Source: htpp://img.brainkart.com]

A laser source (i.e. He–Ne, Nd : YAG, krypton ion) is utilized to provide sufficient optical power at a single wavelength together with a suitable instrument to measure the response from the detector. In order to avoid inaccuracies in the measurement resulting from scattered light which may be trapped in the fiber, cladding mode strippers are placed before and after the scattering cell. These devices remove the light propagating in the cladding so that the measurements are taken only using the light guided by the fiber core. Also, to avoid reflections contributing to the optical signal within the cell, the output fiber end is index matched using either a fluid or suitable surface.

The loss due to scattering αsc is given by:

$$\alpha_{sc} = \frac{10}{l(\text{km})} \log_{10}\left(\frac{P_{opt}}{P_{opt} - P_{sc}}\right) \text{dB km}^{-1} \quad (4.3)$$

where *l*(km) is the length of the fiber contained within the scattering cell, *P*opt is the optical power propagating within the fiber at the cell and *P*sc is the optical power scattered from the short length of fiber *l* within the cell. As *P*opt>>*P*sc, then the logarithm in Eq. (4.3) may be expanded to give:

$$\alpha_{sc} = \frac{4.343}{l(\text{km})}\left(\frac{P_{sc}}{P_{opt}}\right) \text{dB km}^{-1} \quad (4.4)$$

Since the measurements of length are generally in centimeters and the optical power is normally registered in volts, Eq. (4.4) can be written as:

$$\alpha_{sc} = \frac{4.343 \times 10^5}{l(\text{cm})}\left(\frac{V_{sc}}{V_{opt}}\right) \text{dB km}^{-1} \quad (4.5)$$

where *V*sc and *V*opt are the voltage readings corresponding to the scattered optical power and the total optical power within the fiber at the cell. The relative experimental accuracy (i.e. repeatability) for scatter loss measurements is in the range ±0.2 dB using the solar cell cube and around 5% with the integrating sphere. However, it must be noted that the absolute accuracy of the measurements is somewhat poorer, being dependent on the calibration of the scattering cell and the mode distribution within a multimode fiber.

4. Fiber Dispersion Measurements

Dispersion measurements give an indication of the distortion to optical signals as they propagate down optical fibers. The delay distortion which, for example, leads to the broadening of transmitted light pulses limits the information-carrying capacity of the fiber. The measurement of dispersion allows the bandwidth of the fiber to be determined. Therefore, besides attenuation, dispersion is the most important transmission characteristic of an optical fiber. there are three major mechanisms which produce dispersion in optical fibers (material dispersion, waveguide dispersion and intermodal dispersion). The importance of these different mechanisms to the total fiber dispersion is dictated by the fiber type. For instance, in multimode fibers (especially step index), intermodal dispersion tends to be the dominant mechanism, whereas in single-mode fibers intermodal dispersion is nonexistent as only a single mode is allowed to propagate. In the single-mode case, the dominant dispersion mechanism is chromatic (i.e. intramodal dispersion). The dominance of intermodal dispersion in multimode fibers makes it essential that dispersion measurements on these fibers are performed only when the equilibrium mode distribution has been established within the fiber, otherwise inconsistent results will be obtained. Therefore devices such as mode scramblers or filters must be utilized in order to simulate the steady state mode distribution.

Dispersion effects may be characterized by taking measurements of the impulse response of the fiber in the time domain, or by measuring the baseband frequency response in the frequency domain. If it is assumed that the fiber response is linear with regard to power, a mathematical description in the time domain for the optical output power $P_o(t)$ from the fiber may be

obtained by convoluting the power impulse response $h(t)$ with the optical input power $P_i(t)$ as:

$$P_o(t) = h(t) * P_i(t) \tag{4.6}$$

where the asterisk * denotes convolution. The convolution of $h(t)$ with $P_i(t)$ shown in Eq. (4.6) may be evaluated using the convolution integral where:

$$P_o(t) = \int_{-\infty}^{\infty} P_i(t-x)h(x)\,dx \tag{4.7}$$

In the frequency domain the power transfer function $H(\omega)$ is the Fourier transform of $h(t)$ and therefore by taking the Fourier transforms of all the functions in Eq. (4.6) we obtain:

$$\mathcal{P}_o(\omega) = H(\omega)\mathcal{P}_i(\omega) \tag{4.8}$$

A. Time domain measurement

The most common method for time domain measurement of pulse dispersion in multimode optical fibers is illustrated in Figure 4.9. Short optical pulses (100 to 400 ps) are launched into the fiber from a suitable source (e.g. A1GaAs injection laser) using fast driving electronics. The pulses travel down the length of fiber under test (around 1 km) and are broadened due to the various dispersion mechanisms. However, it is possible to take measurements of an isolated dispersion mechanism by, for example, using a laser with a narrow spectral width when testing a multimode fiber. In this case the chromatic dispersion is negligible and the measurement thus reflects only intermodal dispersion.

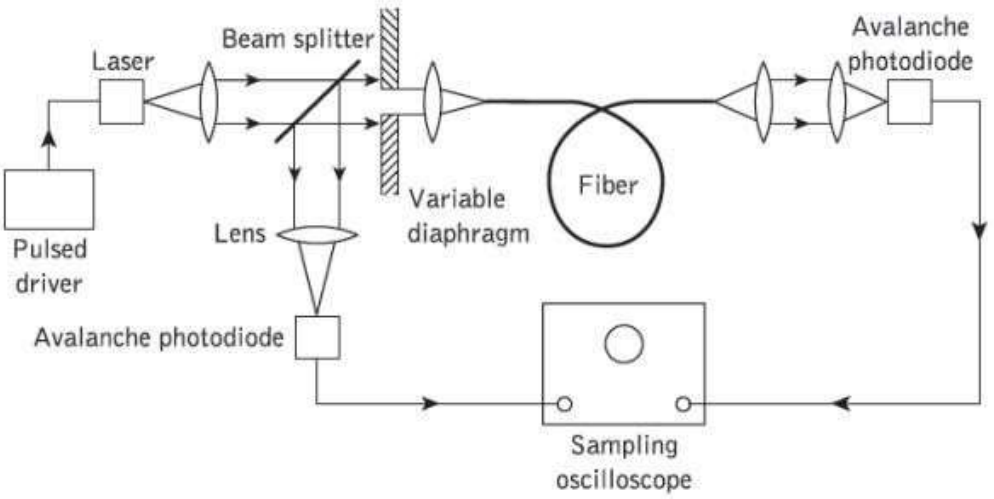

Figure 4.9 Experimental arrangement for making multimode fiber dispersion measurements in the time domain.

[Source: htpp://img.brainkart.com]

The pulses are received by a high-speed photodetector (i.e. avalanche photodiode) and are displayed on a fast sampling oscilloscope. A beam splitter is utilized for triggering the oscilloscope and for input pulse measurement. After the initial measurement of output pulse width, the long fiber length may be cut back to a short length and the measurement repeated in order to obtain the effective input pulse width. The fiber is generally cut back to the lesser of 10 m or 1% of its original length . As an alternative to this cut-back technique, the insertion or substitution method similar to that used in fiber loss measurement can be employed. This method has the benefit of being nondestructive and only slightly less accurate than the cut-back technique.

The fiber dispersion is obtained from the two pulse width measurements which are taken at any convenient fraction of their amplitude. If *P*i(*t*) and*P*o(*t*) of Eq. (4.6) are assumed to have a Gaussian shape then Eq. (4.6) may be written in the form:

$$\tau_o^2(3\text{ dB}) = \tau^2(3\text{ dB}) + \tau_i^2(3\text{ dB}) \qquad (4.9)$$

where τi(3 dB) and τo(3 dB) are the 3 dB pulse widths at the fiber input and output, respectively, and τ (3 dB) is the width of the fiber impulse response again measured at half the maximum amplitude. Hence the pulse dispersion in the fiber (commonly referred to as the pulse broadening when considering the 3 dB pulse width) in ns km^{-1} is given by:

$$\tau(3\text{ dB}) = \frac{(\tau_o^2(3\text{ dB}) - \tau_i^2(3\text{ dB}))^{\frac{1}{2}}}{L}\ \text{ns km}^{-1} \qquad (4.10)$$

where τ(3 dB), τi(3 dB) and τo(3 dB) are measured in ns and *L* is the fiber length in km.

It must be noted that if a long length of fiber is cut back to a short length in order to take the input pulse width measurement, then *L* corresponds to the difference between the two fiber lengths in km.

B. Frequency domain measurement

Frequency domain measurement is the preferred method for acquiring the bandwidth of multimode optical fibers. This is because the baseband frequency response *H*(ω) of the fiber may be obtained directly from these measurements using Eq. (4.8) without the need for any assumptions of Gaussian shape, or alternatively, the mathematically complex deconvolution of Eq. (4.8) which is necessary with measurements in the time domain. Thus the optical bandwidth of a multimode fiber is best obtained from frequency domain measurements.

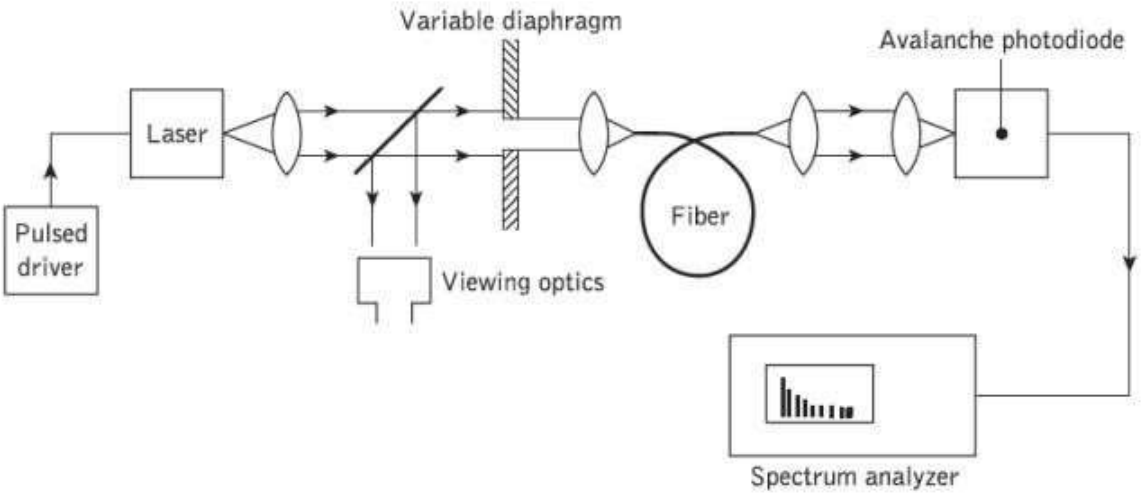

Figure 4.10 Experimental setup for making fiber dispersion measurements in the frequency domain using a pulsed laser source

[Source: htpp://img.brainkart.com]

One of two frequency domain measurement techniques is generally used. The first utilizes a similar pulsed source to that employed for the time domain measurements shown in Figure 4.9. However, the sampling oscilloscope is replaced by a spectrum analyzer which takes the Fourier transform of the pulse in the time domain and hence displays its constituent frequency components. The experimental arrangement is illustrated in Figure 4.10. Comparison of the spectrum at the fiber output Po(ω) with the spectrum at the fiber input Pi(ω) provides the baseband frequency response for the fiber under test where:

$$H(\omega) = \frac{\mathcal{P}_o(\omega)}{\mathcal{P}_i(\omega)} \qquad (4.11)$$

The second technique involves launching a sinusoidally modulated optical signal at different selected frequencies using a sweep oscillator. Therefore the signal energy is concentrated in a very narrow frequency band in the baseband region, unlike the pulse measurement method where the signal energy is spread over the entire baseband region.

5. Fiber Refractive Index Profile Measurements

The refractive index profile of the fiber core plays an important role in characterizing the properties of optical fibers. It allows determination of the fiber's numerical aperture and the number of modes propagating within the fiber core, while largely defining any intermodal and/or profile dispersion caused by the fiber. Hence a detailed knowledge of the refractive index profile enables the impulse response of the fiber to be predicted.

Also, as the impulse response and consequently the information-carrying capacity of the fiber is strongly dependent on the refractive index profile, it is essential that the fiber manufacturer is able to produce particular profiles with great accuracy, especially in the case of graded index fibers (i.e. optimum profile). There is therefore a requirement for accurate measurement of the refractive index profile. These measurements may be performed using a number of different techniques each of which exhibit certain advantages and drawbacks.

In this section we will discuss some of the more popular methods which may be relatively easily interpreted theoretically, without attempting to review all the possible techniques which have been developed.

A. Interferometric methods

Interference microscopes (e.g. Mach–Zehnder, Michelson) have been widely used to determine the refractive index profiles of optical fibers. The technique usually involves the preparation of a thin slice of fiber (slab method) which has both ends accurately polished to obtain square (to the fiber axes) and optically

flat surfaces. The slab is often immersed in an index-matching fluid, and the assembly is examined with an interference microscope. Two major methods are then employed, using either a transmitted light interferometer or a reflected light interferometer.

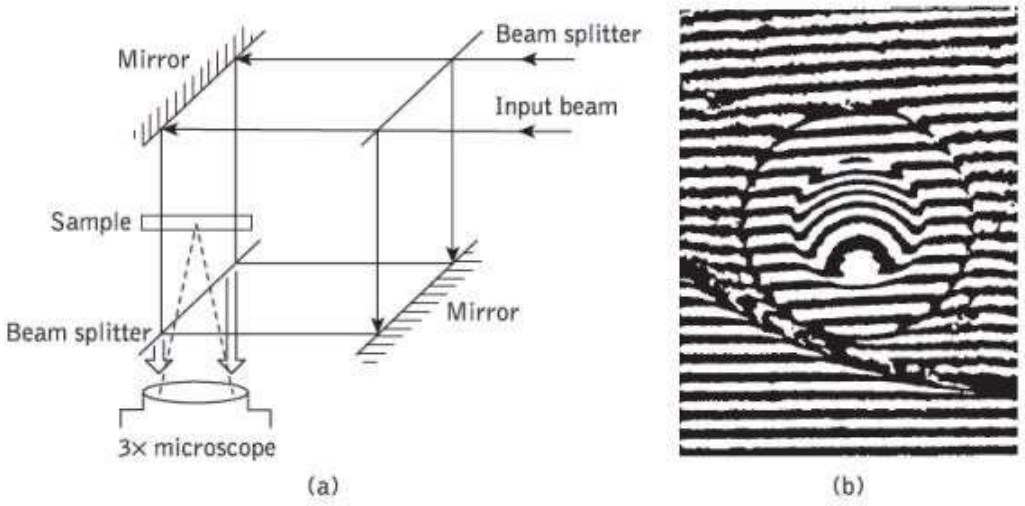

Figure 4.11 (a) The principle of the Mach–Zehnder interferometer. (b) The interference fringe pattern obtained with an interference microscope from a graded index fiber

[Source: htpp://img.brainkart.com]

In both cases light from the microscope travels normal to the prepared fiber slice faces (parallel to the fiber axis), and differences in refractive index result in different optical path lengths. This situation is illustrated in the case of the Mach–Zehnder interferometer in Figure 4.11(a). When the phase of the incident light is compared with the phase of the emerging light, a field of parallel interference fringes is observed. A photograph of the fringe pattern may then be taken, an example of which is shown in Figure 4.11(a).

The fringe displacements for the points within the fiber core are then measured using as reference the parallel fringes outside the fiber core (in the fiber cladding). The refractive index difference between a point in the fiber core (e.g. the core axis) and the cladding can be obtained from the fringe shift q, which corresponds to a number of fringe displacements.

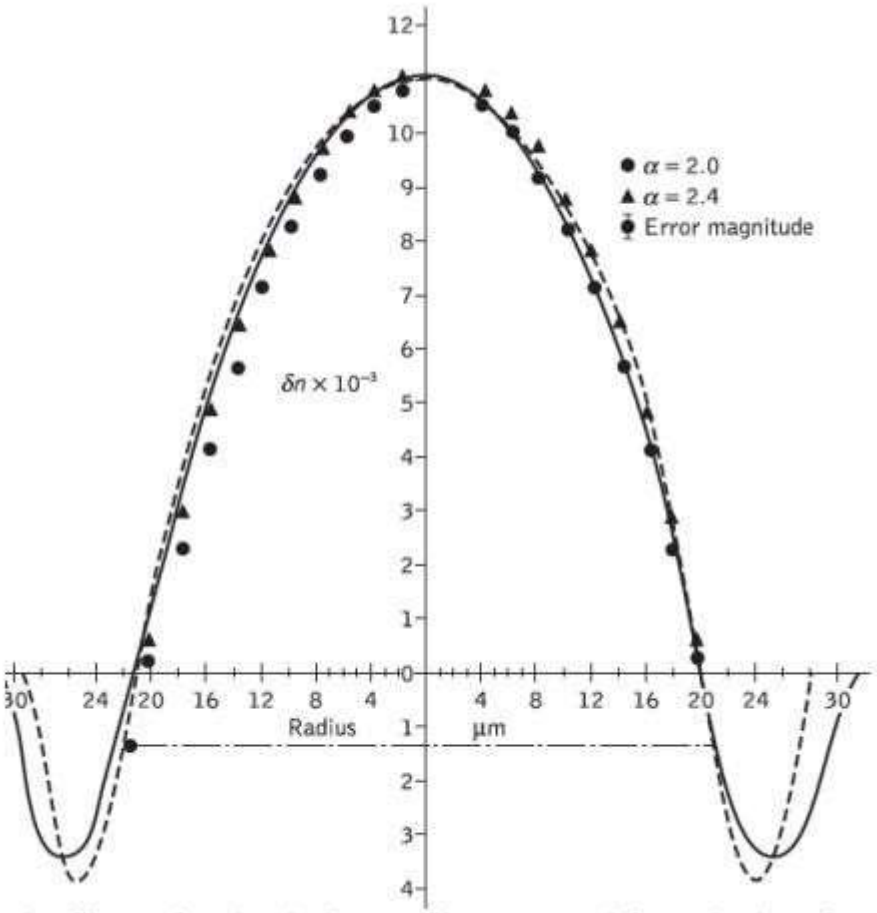

Figure 4.12 The fiber refractive index profile computed from the interference pattern

This difference in refractive index δn is given by:

$$\delta n = \frac{q\lambda}{x} \tag{4.12}$$

where x is the thickness of the fiber slab and λ is the incident optical wavelength. The slab method gives an accurate measurement of the refractive index profile, although computation of the individual points is somewhat tedious unless an automated technique is used.

Figure 4.13 shows the experimental setup used to observe an IGA response using a nonlinear optical loop mirror interferometer. It consists of a laser source and a combination of optical lenses and mirrors where a beam splitter separates the signal creating the delayed path. The two optical signals (i.e. original and delayed signals) combine at a point where a photorefractive

crystal is placed which is the mixing element employed in this method. Several crystalline material systems, known as photorefractive crystals, can be used to produce a diffraction grating in order to implement IGA. Photorefraction is, however, an electro-optic phenomenon in which the local index of refraction is modified by spatial variations of the light intensity.

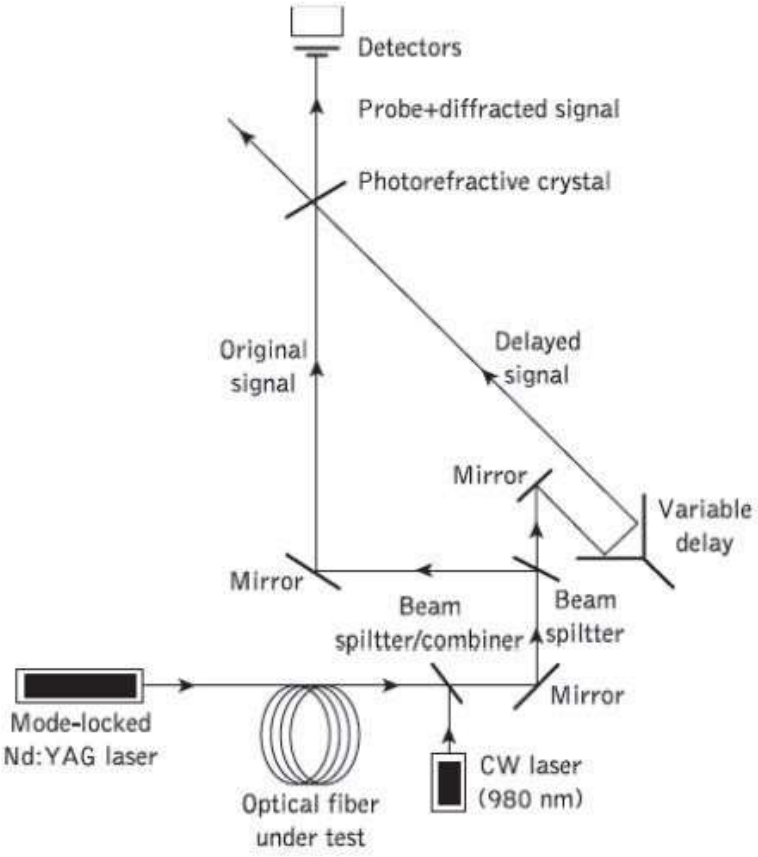

Figure 4.13 Experimental setup for the measurement of the refractive index of silica fiber using the induced-grating autocorrelation function technique

B. Near-field scanning method

The near-field scanning or transmitted near-field method utilizes the close resemblance that exists between the near-field intensity distribution and the refractive index profile, for a fiber with all the guided modes equally

illuminated. It provides a reasonably straightforward and rapid method for acquiring the refractive index profile.

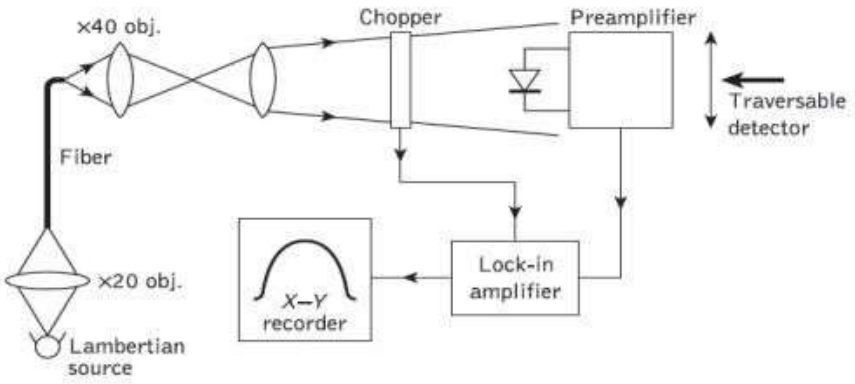

Figure 4.14 Experimental setup for the near-field scanning measurement of the refractive index profile

When a diffuse Lambertian source (e.g. tungsten filament lamp or LED) is used to excite all the guided modes then the near-field optical power density at a radius *r* from the core axis *P*D(*r*) may be expressed as a fraction of the core axis near-field optical power density *P*D(0) following:

$$\frac{P_D(r)}{P_D(0)} = C(r,z)\left[\frac{n_1^2(r) - n_2^2}{n_1^2(0) - n_2^2}\right] \tag{4.13}$$

where *n*1(0) and *n*1(*r*) are the refractive indices at the core axis and at a distance *r* from the core axis respectively, *n*2 is the cladding refractive index and *C*(*r*, *z*) is a correction factor. The correction factor which is incorporated to compensate for any leaky modes present in the short test fiber may be determined analytically.

The transmitted near-field approach is, however, not similarly recommended for single-mode fiber. An experimental configuration is shown in Figure 4.14. The output from a Lambertian source is focused onto the end of the fiber using a microscope objective lens. A magnified image of the fiber output end is displayed in the plane of a small active area photodetector (e.g. silicon *p–i–n* photodiode). The photodetector which scans the field transversely receives

amplification from the phase-sensitive combination of the optical chopper and lock-in amplifier. Hence the profile may be plotted directly on an *X*–*Y* recorder. However, the profile must be corrected with regard to $C(r, z)$ as illustrated in Figure 4.15(a) which is very time consuming. Both the scanning and data acquisition can be automated with the inclusion of a minicomputer.

The test fiber is generally 2 m in length to eliminate any differential mode attenuation and mode coupling. A typical refractive index profile for a practical step index fiber measured by the near-field scanning method is shown in Figure 4.15(b). It may be observed that the profile dips in the center at the fiber core axis. This dip was originally thought to result from the collapse of the fiber preform before the fiber is drawn in the manufacturing process but has been shown to be due to the layer structure inherent at the deposition stage.

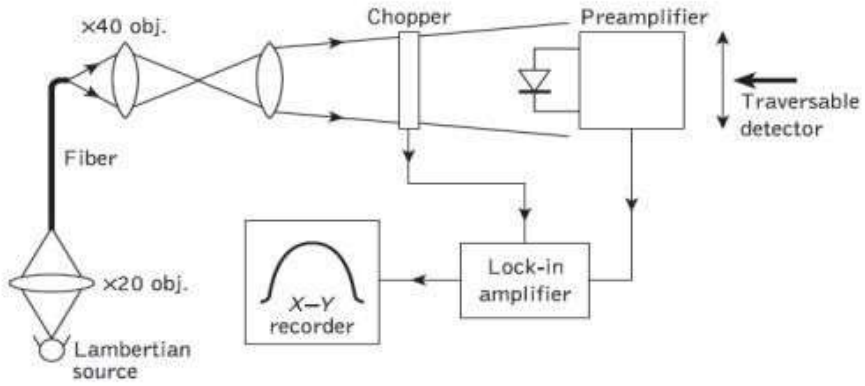

Figure 4.14 Experimental setup for the near-field scanning measurement of the refractive index profile

When a diffuse Lambertian source (e.g. tungsten filament lamp or LED) is used to excite all the guided modes then the near-field optical power density at a radius r from the core axis $PD(r)$ may be expressed as a fraction of the core axis near-field optical power density $PD(0)$ following:

[Source: htpp://img.brainkart.com]

6. Fiber Cutoff Wavelength Measurements

A multimode fiber has many cutoff wavelengths because the number of bound propagating modes is usually large. For example, considering a parabolic refractive index graded fiber, the number of guided modes *M*g is:

$$M_g = \left(\frac{\pi a}{\lambda}\right)^2 (n_1^2 - n_2^2) \qquad (4.14)$$

where *a* is the core radius and *n*1 and *n*2 are the core peak and cladding indices respectively. It may be observed from Eq. (4.14) that operation at longer wavelengths yields fewer guided modes. Therefore it is clear that as the wavelength is increased, a growing number of modes are cutoff where the cutoff wavelength of a LP*lm* mode is the maximum wavelength for which the mode is guided by the fiber.

Usually the cutoff wavelength refers to the operation of single-mode fiber in that it is the cutoff wavelength of the LP11 mode (which has the longest cutoff wavelength) which makes the fiber single moded when the fiber diameter is reduced to 8 or 9 μm. Hence the cutoff wavelength of the LP11 is the shortest wavelength above which the fiber exhibits single-mode operation and it is therefore an important parameter to measure.

The theoretical value of the cutoff wavelength can be determined from the fiber refractive index profile. Because of the large attenuation of the LP11 mode near cutoff, however, the parameter which is experimentally determined is called the effective cutoff wavelength, which is always smaller than the theoretical cutoff wavelength by as much as 100 to 200 nm. It is this effective cutoff wavelength which limits the wavelength region for which the fiber is ‘effectively’ single-mode.

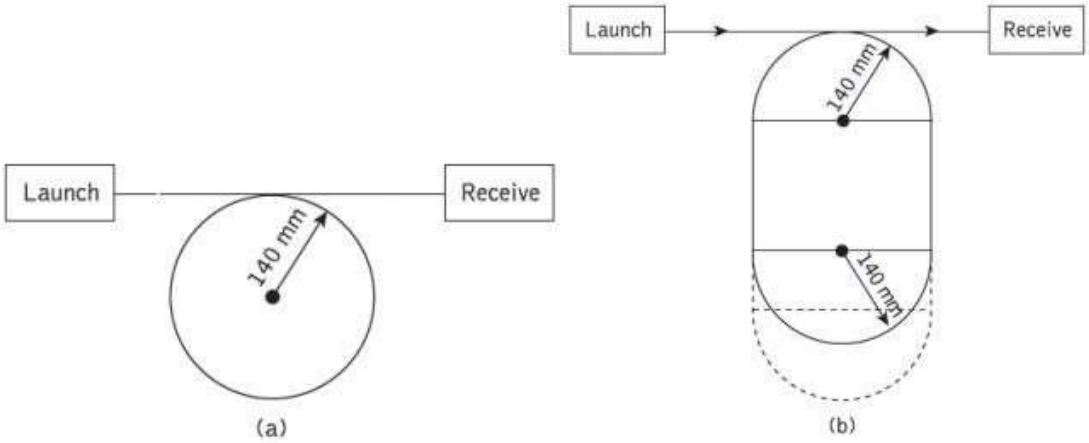

Figure 4.16 Configurations for the measurement of uncabled fiber cutoff wavelength: (a) single turn; (b) split mandrell

[Source: htpp://img.brainkart.com]

In the bending-reference technique the power Ps(λ) transmitted through the fiber sample in the configurations shown in Figure 4.16 is measured as a function of wavelength. Thus the quantity Ps(λ) corresponds to the total power, including launched higher order modes, of the ITU-T definition for cutoff wavelength. Then keeping the launch conditions fixed, at least one additional loop of sufficiently small radius (60 mm or less) is introduced into the test sample to act as a mode filter to suppress the secondary LP11 mode without attenuating the fundamental mode at the effective cutoff wavelength. In this case the smaller transmitted spectral power Pb(λ) is measured which corresponds to the fundamental mode power referred to in the definition. The bend attenuation ab(λ) comprising the level difference between the total power and the fundamental power is calculated as:

$$a_b(\lambda) = 10 \log_{10} \frac{P_s(\lambda)}{P_b(\lambda)} \qquad (4.15)$$

The bend attenuation characteristic exhibits a peak in the wavelength region where the radiation losses resulting from the small loop are much higher for the LP11 mode than for the LP01 fundamental mode, as illustrated in Figure 4.17.

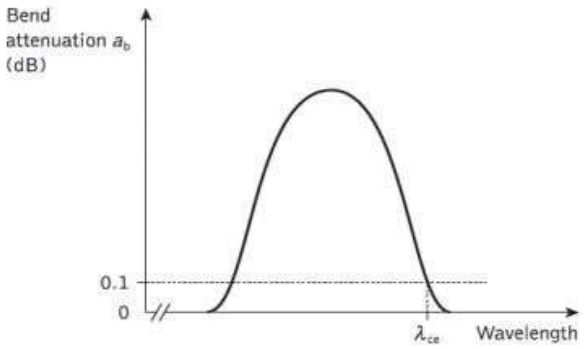

Figure 4.17 Bend attenuation against wavelength in the bending method for the measurement of cutoff wavelength λce

[Source: htpp://img.brainkart.com]

It should be noted that the shorter wavelength side of the attenuation maximum corresponds to the LP11 mode, being well confined in the fiber core, and hence negligible loss is induced by the 60 mm diameter loop, whereas on the longer wavelength side the LP11 mode is not guided in the fiber and therefore, assuming that the loop diameter is large enough to avoid any curvature loss to the fundamental mode, there is also no increase in loss.

The relative attenuation *a*m(λ) or level difference between the powers launched into the multimode and single-mode fibers may be computed as:

$$a_m(\lambda) = 10 \log_{10} \frac{P_s(\lambda)}{P_m(\lambda)} \qquad (4.16)$$

7. Fiber Numerical Aperture Measurements

The numerical aperture is an important optical fiber parameter as it affects characteristics such as the light-gathering efficiency and the normalized frequency of the fiber (*V*). This in turn dictates the number of modes propagating within the fiber (also defining the singlemode region) which has consequent effects on both the fiber dispersion (i.e. intermodal) and, possibly, the fiber attenuation (i.e. differential attenuation of modes). The numerical aperture (*NA*) is defined for a step index fiber as:

$$NA = \sin \theta_a = (n_1^2 - n_2^2)^{\frac{1}{2}} \tag{4.17}$$

where Θa is the maximum acceptance angle, $n1$ is the core refractive index and $n2$ is the cladding refractive index.

It is assumed that the light is incident on the fiber end face from air with a refractive index ($n0$) of unity. Although Eq. (4.17) may be employed with graded index fibers, the numerical aperture thus defined represents only the local *NA* of the fiber on its core axis (the numerical aperture for light incident at the fiber core axis). The graded profile creates a multitude of local *NA*s as the refractive index changes radially from the core axis

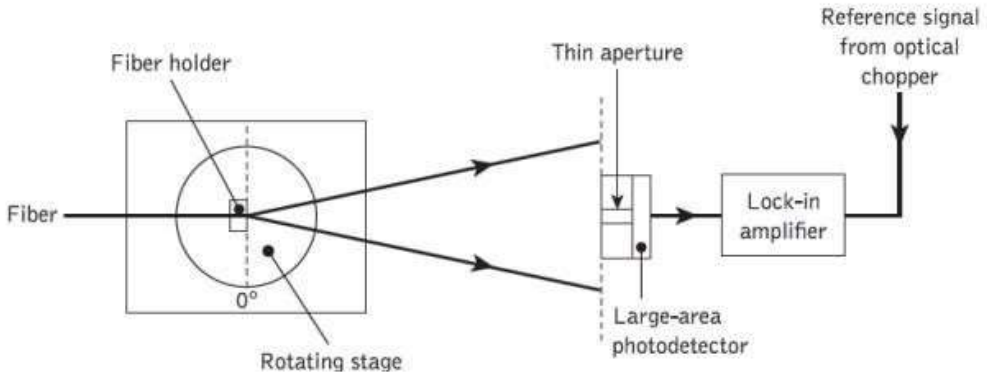

Figure 4.18 Fiber numerical aperture measurement using a scanning photodetector and a rotating stage

[Source: htpp://img.brainkart.com]

For the general case of a graded index fiber these local numerical apertures NA(r) at different radial distances r from the core axis may be defined by:

$$NA(r) = \sin \theta_a(r) = (n_1^2(r) - n_2^2)^{\frac{1}{2}} \tag{4.18}$$

Therefore, calculations of numerical aperture from refractive index data are likely to be less accurate for graded index fibers than for step index fibers unless the complete refractive index profile is considered. The numerical aperture may be determined by calculation.

` An example of an experimental arrangement with a rotating stage is shown in Figure 4.18. A 2 m length of the graded index fiber has its faces prepared in order to ensure square smooth terminations.

The fiber output end is then positioned on the rotating stage with its end face parallel to the plane of the photodetector input, and so that its output is perpendicular to the axis of rotation. Light at a wavelength of 0.85 μm is launched into the fiber at all possible angles (overfilling the fiber) using an optical system similar to that used in the spot attenuation measurements.

The photodetector, which may be either a small-area device or an apertured large-area device, is placed 10 to 20 cm from the fiber and positioned in order to obtain a maximum signal with no rotation (0°). Hence when the rotating stage is turned the limits of the far-field pattern may be recorded. The output power is monitored and plotted as a function of angle, the maximum acceptance angle being obtained when the power drops to 5% of the maximum intensity. Thus the numerical aperture of the fiber can be obtained from Eq. (4.17).

A less precise measurement of the numerical aperture can be obtained from the far-field pattern by trigonometric means. The experimental apparatus is shown in Figure 4.19.

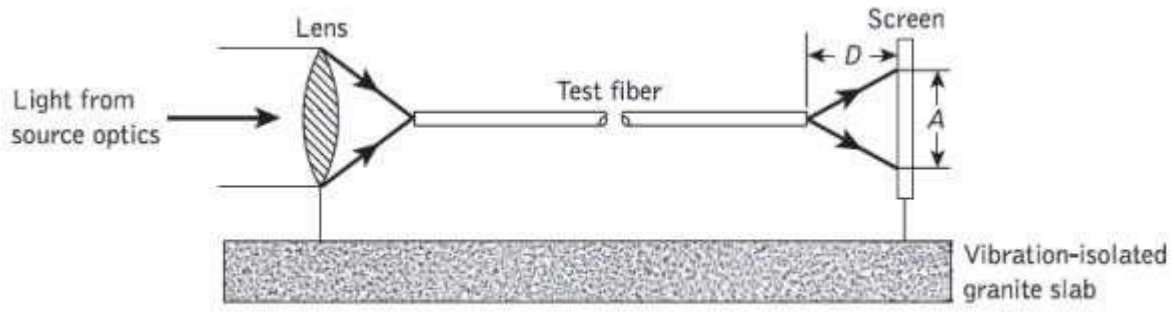

Figure 4.19 Apparatus for trigonometric fiber numerical aperture measurement

[Source: htpp://img.brainkart.com]

where the end prepared fiber is located on an optical base plate or slab. Again light is launched into the fiber under test over the full range of its numerical aperture, and the farfield pattern from the fiber is displayed on a screen which is positioned a known distance *D* from the fiber output end face. The test fiber is then aligned so that the optical intensity on the screen is maximized. Finally, the pattern size on the screen *A* is measured using a calibrated vernier caliper. The numerical aperture can be obtained from simple trigonometrical relationships where:

$$NA = \sin\theta_a = \frac{A/2}{[(A/2)^2 + D^2]^{\frac{1}{2}}} = \frac{A}{(A^2 + 4D^2)^{\frac{1}{2}}} \qquad (4.19)$$

It must be noted that the accuracy of this measurement technique is dependent upon the visual assessment of the far-field pattern from the fiber. The above measurement techniques are generally employed with multimode fibers only, as the far-field patterns from single-mode fibers are affected by diffraction phenomena

8. Fiber Diameter Measurements

A. Outer diameter

It is essential during the fiber manufacturing process (at the fiber drawing stage) that the fiber outer diameter (cladding diameter) is maintained constant to within 1%. Any diameter variations may cause excessive radiation losses and make accurate fiber–fiber connection difficult. Hence on-line diameter measurement systems are required which provide accuracy better than 0.3% at a measurement rate greater than 100 Hz (i.e. a typical fiber drawing velocity is 1 ms -1). Use is therefore made of noncontacting optical methods such as fiber image projection and scattering pattern analysis.

The most common on-line measurement technique uses fiber image projection (shadow method) and is illustrated in Figure 4.20. In this method a laser beam is swept at a constant velocity transversely across the fiber and a measurement is made of the time interval during which the fiber intercepts the beam and casts a shadow on a photodetector.

In the apparatus shown in Figure 4.20 the beam from a laser operating at a wavelength of 0.6328 μm is collimated using two lenses ($G1$ and $G2$). It is then reflected off two mirrors ($M1$ and $M2$), the second of which ($M2$) is driven by a galvanometer which makes it rotate through a small angle at a constant angular velocity before returning to its original starting position. Therefore, the laser beam which is focused in the plane of the fiber by a lens ($G3$) is swept across the fiber by the oscillating mirror, and is incident on the photodetector unless it is blocked by the fiber. The velocity ds/dt of the fiber shadow thus created at the photodetector is directly proportional to the mirror velocity $d\phi/dt$ following:

$$\frac{ds}{dt} = l\frac{d\phi}{dt} \quad (14.31) \qquad (4.20)$$

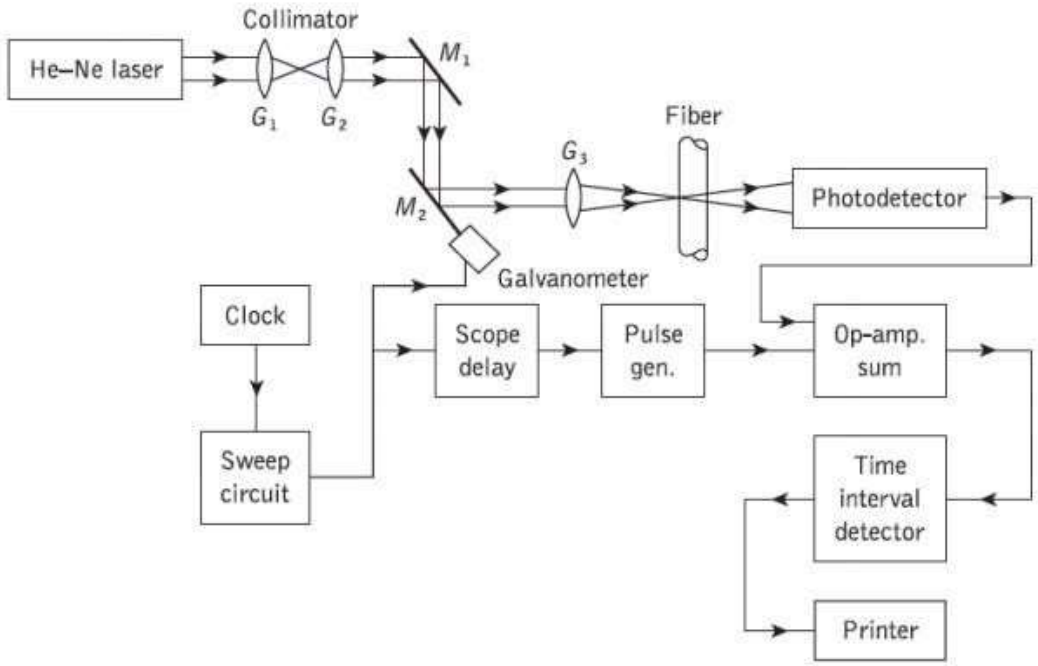

Figure 4.20 The shadow method for the on-line measurement of the fiber outer diameter.

[Source: htpp://img.brainkart.com]

where *l* is the distance between the mirror and the photodetector. Furthermore, the shadow is registered by the photodetector as an electrical pulse of width *We* which is related to the fiber outer diameter *do* as:

$$d_o = W_e\frac{ds}{dt} \qquad (4.21)$$

Thus the fiber outer diameter may be quickly determined and recorded on the printer. The measurement speed is largely dictated by the inertia of the mirror rotation and its accuracy by the rise time of the shadow pulse.

Other on-line measurement methods, enabling faster diameter measurements, involve the analysis of forward or backward far-field patterns which are produced when a plane wave is incident transversely on the fiber. These techniques generally require measurement of the maxima in the center portion of the scattered pattern from which the diameter can be calculated after detailed mathematical analysis. They tend to give good accuracy (e.g. ±0.25 μm) even

though the theory assumes a perfectly circular fiber cross-section. Also, for step index fibers the analysis allows determination of the core diameter, and core and cladding refractive indices. Measurements of the fiber outer diameter after manufacture (off-line) may be performed using a micrometer or dial gage. These devices can give accuracies of the order of ±0.5 μm. Alternatively, off-line diameter measurements can be made with a microscope incorporating a suitable calibrated micrometer eyepiece.

B. Core diameter

The core diameter for step index fibers is defined by the step change in the refractive index profile at the core–cladding interface. Therefore the techniques employed for determining the refractive index profile (interferometric, near-field scanning, refracted ray, etc.) may be utilized to measure the core diameter. Graded index fibers present a more difficult problem as, in general, there is a continuous transition between the core and the cladding.

In this case it is necessary to define the core as an area with a refractive index above a certain predetermined value if refractive index profile measurements are used to obtain the core diameter. Core diameter measurement is also possible from the near-field pattern of a suitably illuminated (all guided modes excited) fiber. The measurements may be taken using a microscope equipped with a micrometer eyepiece similar to that employed for off-line outer diameter measurements.

Fundamental Receiver Operation

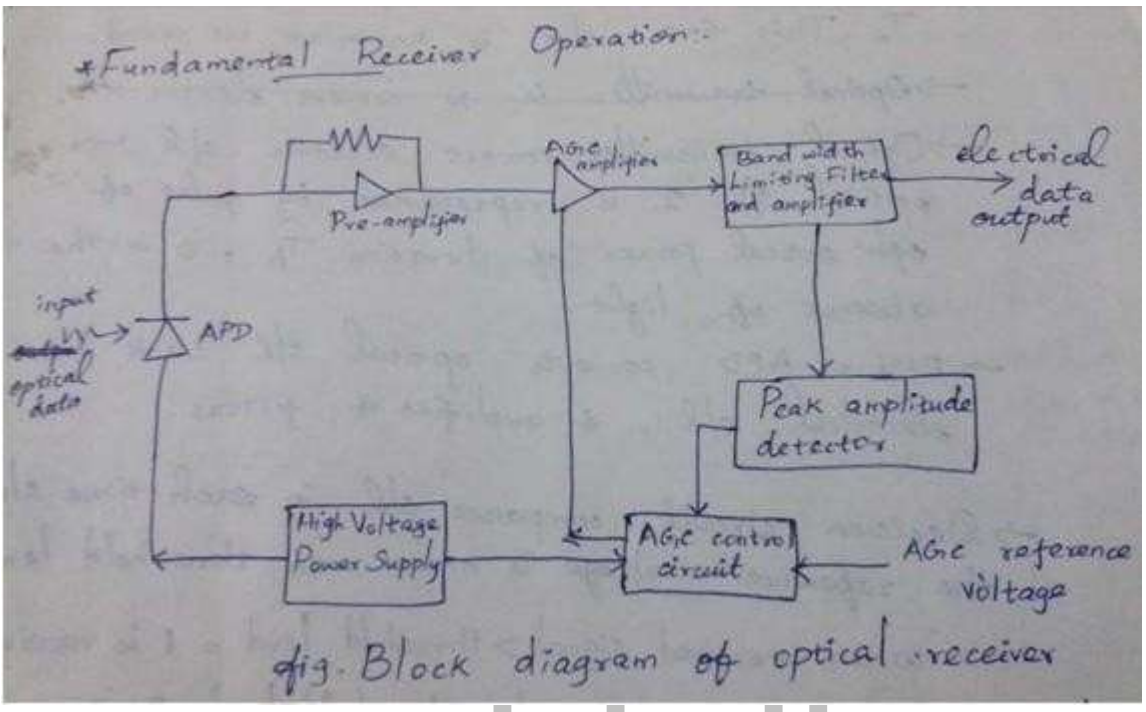

Design of optical receiver is more complicated than optical transmitter because it receives weak and distorted signals. APD produces photocurrent for input optical data. AGC amplifier maintains constant peak amplitude with the help of AGC control circuit. Band limiting filter reduce noise output to desired level.

1. Optical Receiver Operation

✓ A typical digital fiber transmission link is shown in Figure 4.1. The transmitted signal is a two-level binary data stream consisting of either a '0' or a '1' in a *bit period T*b.

✓ The simplest technique for sending binary data is *amplitude-shift keying*, wherein a voltage level is switched between *on* or *off* values.

✓ The resultant signal wave thus consists of a voltage pulse of amplitude *V* when a binary 1 occurs and a zero-voltage-level space when a binary 0 occurs.

Digital Signal Transmission

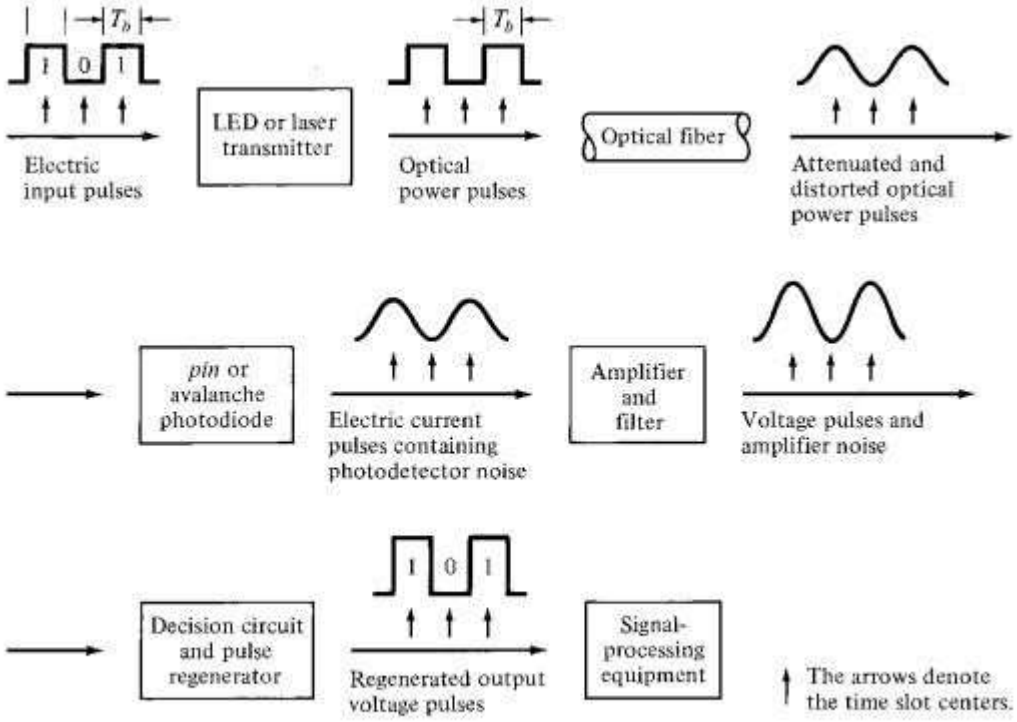

Figure 4.1 Signal path through an optical data link.

[Source: htpp://img.brainkart.com]

✓ An electric current $i(t)$ can be used to modulate directly an optical source to produce an optical output power $P(t)$.

✓ In the optical signal emerging from the transmitter, a '1' is represented by a light pulse of duration Tb, whereas a '0' is the absence of any light.

✓ The optical signal that gets coupled from the light source to the fiber becomes attenuated and distorted as it propagates along the fiber waveguide. Upon reaching the receiver, either a PIN or an APD converts the optical signal back to an electrical format.

✓ A decision circuit compares the amplified signal in each time slot with a *threshold level*.

✓ If the received signal level is greater than the threshold level, a '1' is said to have been received. If the voltage is below the threshold level, a '0' is assumed to have been received.

Pre Amplifier

The receiver amplifiers are the front end preamplifier. The three basic preamplifier structures are:

(1) Low impedance preamplifier

(2) High impedance preamplifier

(3) Trans impedance preamplifier

Advantages of Pre-Amplifier

A preamplifier should satisfy the following requirements: low noise level, high bandwidth, high dynamic range, high sensitive and high gain.

1. **Low Impedance Preamplifier**

- Photo diode operates in to a low impedance amplifier bias or load resistor "R_b" is used to match the amplifier impedance.
- R_b along with the input capacitance of amplifier decides the bandwidth of amplifier.

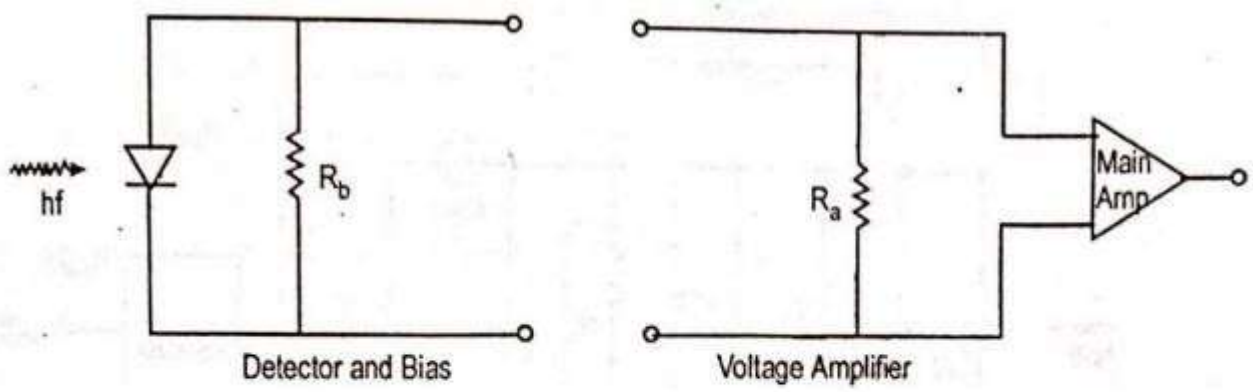

Figure 4.6 Simple Low Impedance Preamplifier Design

$$\text{The total load resistance, } R_{TL} \doteq \frac{R_b R_a}{R_b + R_a}$$

[Source: htpp://img.brainkart.com]

- Low impedance preamplifier can operate over a wide bandwidth but they have poor receiver sensitivity.
- They are used in special short distance application where high sensitivity is not a major concern.

2. High Impedance Preamplifier

- The second configuration consists of a high input impedance amplifier together with a large detector bias resistor (R_a) in order to reduce the effect of thermal noise.
- In high impedance preamplifier, the goal is to reduce all sources of noise to the absolute minimum. This can be achieved by reducing input capacitance through the selection of low capacitance high frequency devices.

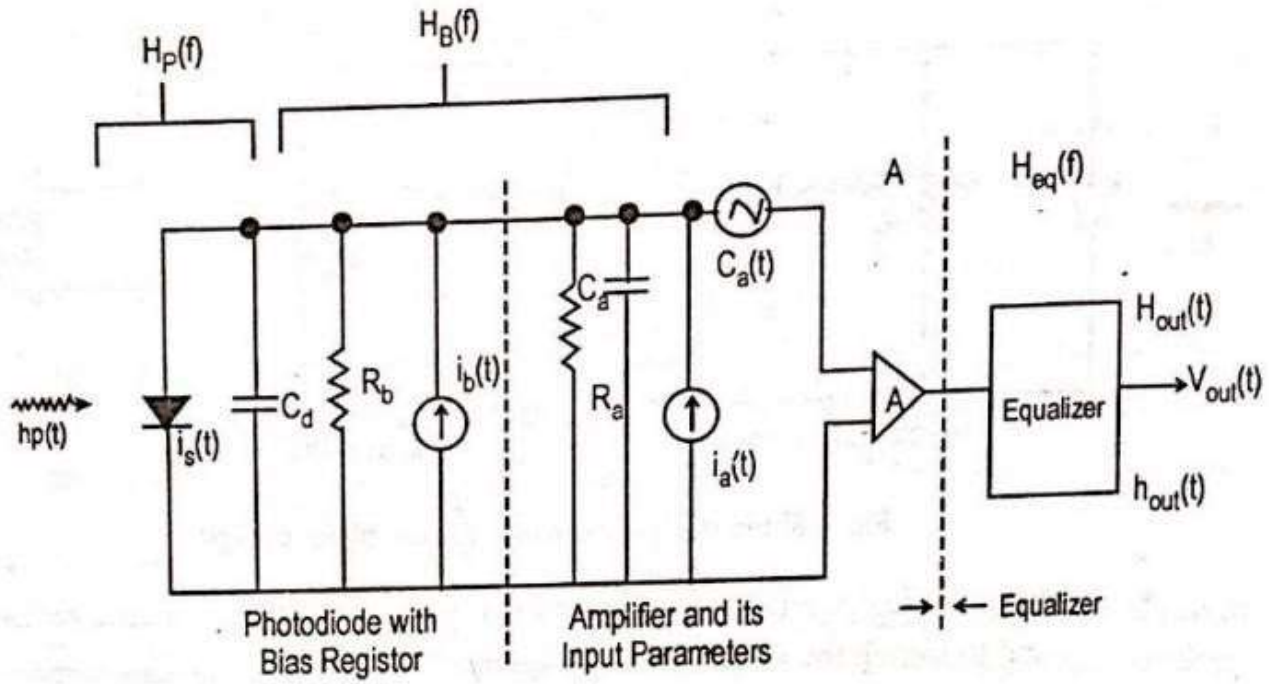

Figure 4.7 Preamplifier Design High Impedance.

[Source: htpp://img.brainkart.com]

- Selecting detectors with low dark currents.
- Minimizing thermal noise of biasing resistors.

- Using high impedance amplifier with large R_b (eg., a dipolar transistor or a field effect transistor (FET)).
- The high impedance procedure a large input RC time constant, the front end bandwidth is less than signal bandwidth. Thus, the input signal is integrated and equalization techniques must be employed to compensate for this.

High Impedance FET Preamplifier

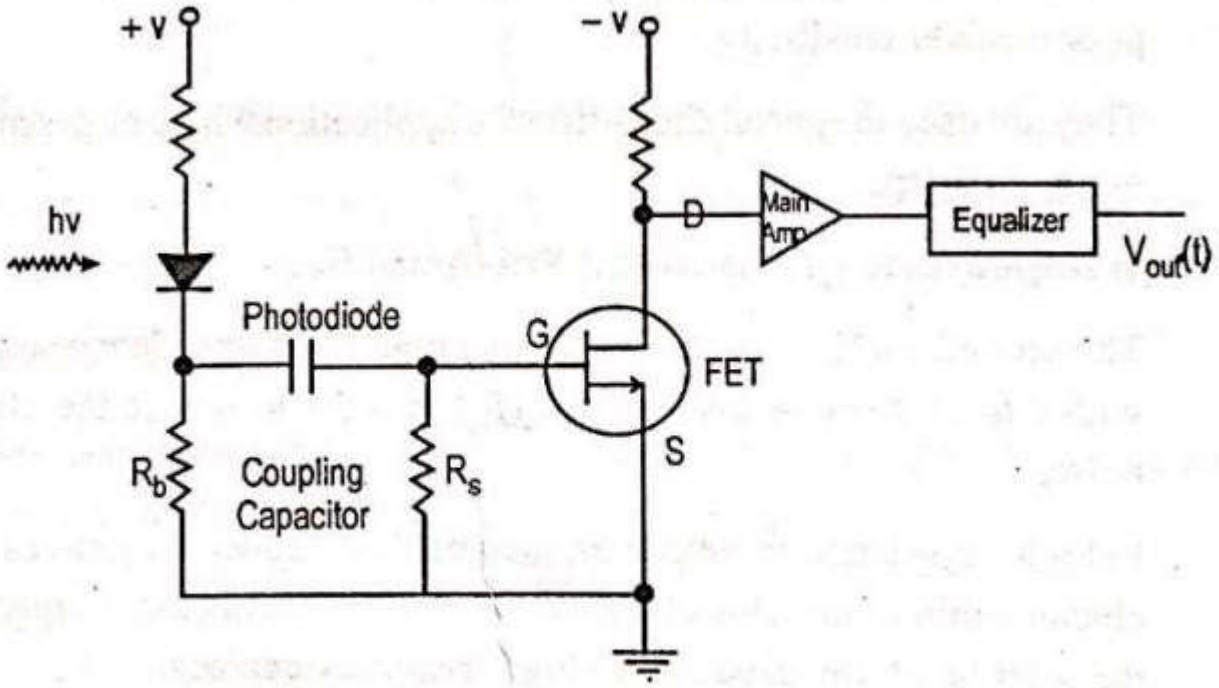

Figure 4.8 High Impedance Preamplifier Design Using FET

[Source: htpp://img.brainkart.com]

- For giga bit per second data rates, the lowest noise receivers are made using GaAs MOSFET (metal oxide semiconductor field effect transistor) preamplifiers.
- At low frequencies, silicon MOSFETs (metal oxide semiconductor field effect transistors) or JFET are generally used.

Basic Noise Sources in the Circuit are:

- Thermal noise associated with FET channel conductance.
- Thermal noise from load or feedback resistor.
- Shot noise due to gate leakage current.
- A fourth noise source is FET $1/f$ noise.
- This ($1/f$ noise) was not include in the above analyses beceause it contributes to the overall noise only at very low bit rates.
- As he amplifier input resistance is very high, the input current noise spectral density S_1 is

$$S_{I,\,FET} = \frac{4K_BT}{R_a} + 2q\,I_{gate}$$

- FET has very large input resistance "R_a" usually greater than $10^6\Omega$ for practical purpose R_e=infinity.

$$S_{I,\,FET} \approx 2\,q\,I_{gate}$$

Where I_{gate} is the channel noise factor.

- The thermal noise of the conducting channel resistance is characterized by the transconductance g_m.
- The voltage noise spectral density is

$$S_E = \frac{4K_BT\Gamma}{g_m}$$

where Γ is the channel-noise factor.

- $\acute{\Gamma}$ is a numerical that accounts for thermal noise and gate included noise plus the correlation between these two noises.
- Thermal noise characteristic equation Ω is a very useful figure of merit for a receiver as it measures

$$W = \frac{1}{q^2 B}\left(S_I + \frac{4K_B T}{R_b} + \frac{S_E}{R^2}\right) I_2 + \frac{(2\pi c)^2}{q^2} S_E I_3 B ,$$

Substituting S_I and S_E, the equalizer output w is

$$W = \frac{1}{q^2 B}\left(2q\, I_{gate} + \frac{4K_B T}{R_b} + \frac{4K_B T\Gamma}{g_m R_b^2}\right) I_2 + \left(\frac{2\pi c}{q}\right)^2 \frac{4K_B T\Gamma}{g_m} I_3 B$$

where $C = C_d + C_{gs} + C_{gd} + C_a$

C_{gs} is the FET gate-source capacitance.

C_{gd} is the FET gate-drain capacitance.

- The 1/*f* noise corner frequency f_c is defined as the frequency at which 1/*f* noise, which dominates the FET noise at low frequencies and has 1/*f*power spectrum, becomes equal frequency channel noise described by Γ.
- To minimize the noise in a high impedance design, the bias resistor shoud be very large. The effect of this is the detector output signal is integrated by the amplifier input resistance.

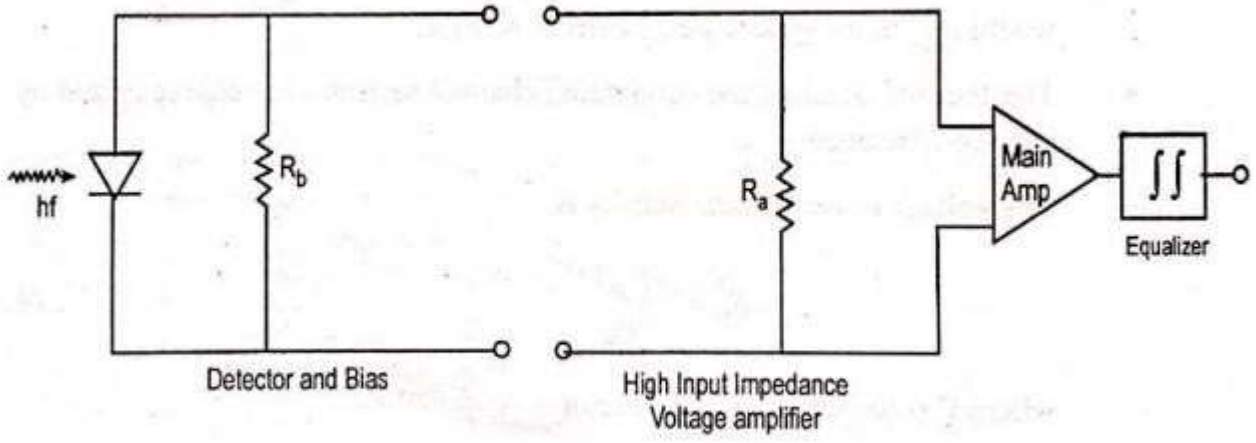

Figure 4.9 Equivalent Circuit to Minimize Noise

[Source: htpp://img.brainkart.com]

- It is compensated by differentiation in the equalizing fitter. This integration differentiation approach is known as the high impedance amplifier design technique.

High Impedance BJT Preamplifier

- The circuit shows a simple bipolar grounded emitter transistor amplifier.
- The input (R_{in}) of a bipolar transistor is given as

$$R_{in} = \frac{K_B T}{q I_{BB}}$$

where I_{BB} is base bias current.

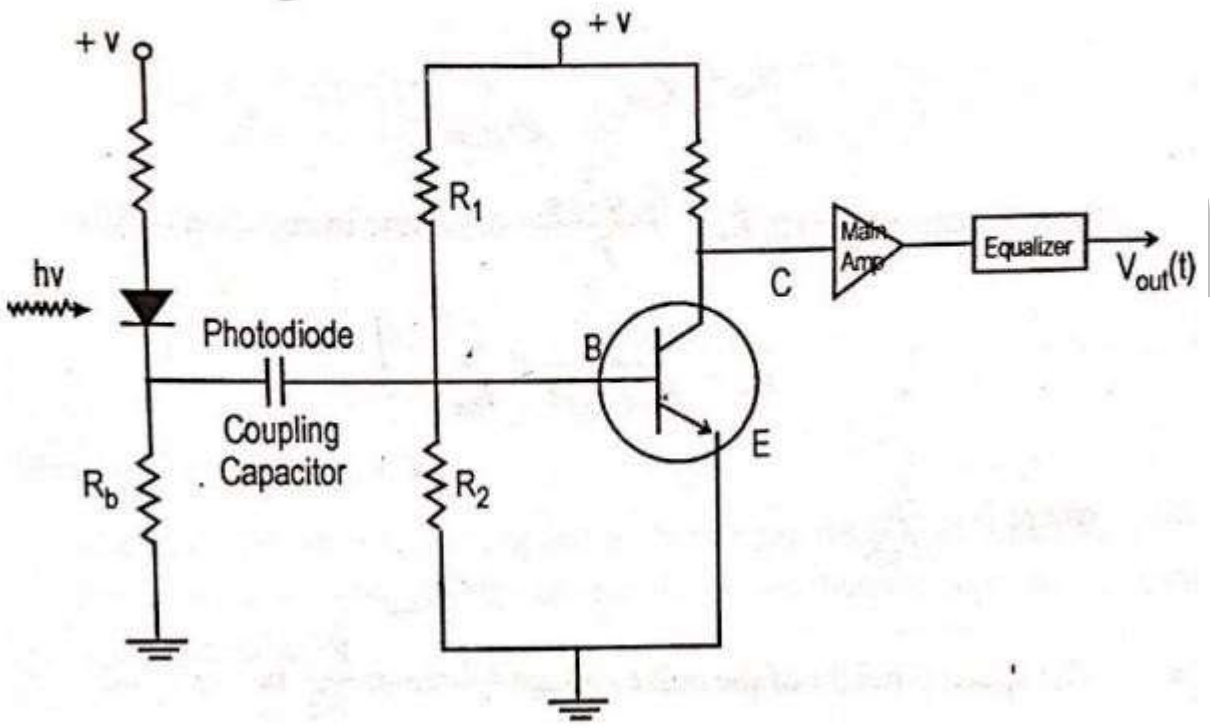

Figure 4.10 High Impedance Preamplifier Design Using FET

[Source: htpp://img.brainkart.com]

- The amplifier input resistance R_a is given by the parallel combination of the bias resistor R_1 and R_2 and the transistor input resistance R_{in}.
- For low noise design ($R_1+R_2>>R_{in}$) $R_a \sim = R_{in}$

- The spectral density (A^2/Hz) of the input noise current source which results from shot noise of the base current is

$$S_I = 2q\ I_{BB}$$

W.K.T $q = \dfrac{K_B T}{R_{in} I_{BB}}$

Now

$$S_I = \frac{2K_B T}{R_{in}}$$

- The transconductance g_m is related to the shot noise and is given by

$$g_m = \frac{q I_c}{K_B I}$$

W.K.T $K_B = \dfrac{R_{in} q I_{BB}}{T}$

Now

$$g_m = \frac{q I_c T}{R_{in} q I_{BB} T} = \frac{\beta}{R_{in}}$$

where $\beta = \dfrac{I_C}{I_{BB}}$.

- The spectral height of the noise voltage source in V^2/Hz is

$$S_E = \frac{2K_B T}{g_m}$$

Where k_b is the boltzmann's constant.

Thermal Noise Characteristic Equation for Receiver Amplifier

- The performance of receiver is expressed by thermal noise characteristic equation (W).

$$W = \frac{1}{q^2 B}\left(S_I + \frac{4K_B T}{R_b} + \frac{S_E}{R^2}\right) I_2 + \frac{(2\pi c)^2}{q^2} S_E I_3 B$$

Substituting R_{in}, S_1,S_E in characteristic equation

$$W = \frac{1}{q^2 B}\left[\frac{2K_B T}{R_{in}} + \frac{4K_B T}{R_b} + \frac{2K_B T}{g_m R^2}\right] I_2 + \frac{(2\pi c)^2}{q^2}\left[\frac{2K_B T}{g_m}\right] I_3 B$$

$$= \frac{2K_B T}{q^2 B}\left[\frac{1}{R_{in}} + \frac{2}{R_b} + \frac{1}{g_m R^2}\right] I_2 + \frac{(2\pi c)^2}{q^2} \cdot \frac{I_3 B}{g_m}$$

$\because B = \frac{1}{T_b}$, $g_m = \frac{\beta}{R_{in}}$ where T_b is bit period

Substitute B & g_m in W, We get:

$$W = \frac{T_b}{q^2} 2K_B T\left[\left(\frac{1}{R_{in}} + \frac{2}{R_b} + \frac{R_{in}}{\beta R^2}\right)\right] I_2 + \frac{(2\pi c)^2}{T_b q^2}\left(\frac{R_{in}}{\beta}\right) I_3$$

If $R_b >> R_a$ then $R_a \approx R_{in}$,

$$W = \frac{2K_B T}{q^2}\left[\frac{T_b}{R_{in}} \cdot \frac{\beta + 1}{\beta} I_2 + \frac{(2\pi c)^2}{\beta T_b} R_{in} I_3\right]$$

Transimpedance Preamplifier

- The transimpedance amplifier is nothing but the low noise high impedance amplifier with a negative feedback 'R_f' resistor, the device therefore operates as a current mode amplifier.

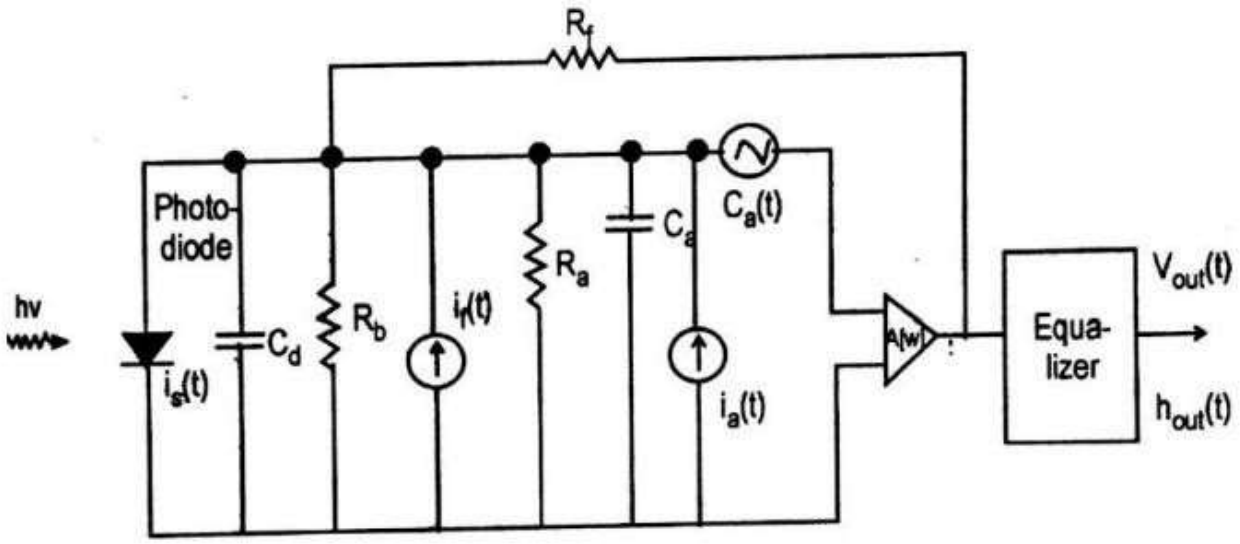

Figure 4.11 Equivalent Circuit of the Transimpedance Receiver Design

[Source: htpp://img.brainkart.com]

- Transimpedance amplifier design overcomes the drawbacks of high impedance amplifier. Such as

(1) For broadband applications, equalization is required.

(2) It has limited dynamic range.

- The thermal noise characteristic 'W_{TZ}' at equalizer output can be found by replacing R_b and R_b'.

$$R_b' = \frac{R_b R_f}{R_b + R_f}$$

- Due to R_b' the thermal noise characteristic equation becomes

$$W_{TZ} = \frac{T_b}{q^2}\left(S_I + \frac{4K_B T}{R_b'} + \frac{S_E}{(R')^2}\right) I_2 + \frac{(2\pi c)^2}{q^2 T_b} S_E I_3$$

where $\frac{1}{R'} = \frac{1}{R} + \frac{1}{R_f} = \frac{1}{R_a} + \frac{1}{R_b} + \frac{1}{R_f}$.

- In practice, $R_f >> R_a$

$$R' \approx R$$

$$W_{TZ} = W_{Hz} + \frac{Tb_4 K_B T}{q^2 R_f} I_2$$

where W_{HZ} is the high-impedance amplifier noise characteristic.

- The thermal noise characteristics are the sum of output noise of a non-feedback amplifier plus the thermal noise associated with the feedback resistance.

Transfer Function of Non-Feedback Amplifier

- The transfer function of non-feedback amplifier is given by

$$H(f) = \frac{AR}{1 + j2\pi RC_f}$$

where A is the frequency-independent gain of the amplifier.

Where $R = \frac{R_a R_b}{R_a + R_b}$, $C = C_a + C_d$

- The bandwidth of non-feedback amplifier is B=1/4RC

Advantages of Transimpedance Amplifier:

(1) Wide dynamic range.

(2) Little or no equalization is required.

(3) Less susceptible to pick up noise, cross talk, EMI.

(4) It is very easily controllable and stable.

(5) Loss sensitivity.

(6) Output resistance is small.